Non-linear dynamics of a drill-string with uncertain model of the bit-rock interaction

T.G. Ritto, Christian Soize, R. Sampaio

Nonlinear dynamics of a drill-string with uncertain model of the bit-rock interaction

T. G. Ritto[a,b], C. Soize[b], R. Sampaio[a]

[a] *PUC-Rio, Department of Mechanical Engineering, Rua Marquês de São Vicente, 225, Gávea, RJ, 22453-900, Brazil, thiagoritto@gmail.com, rsampaio@puc-rio.br*
[b] *Université Paris-Est, Laboratoire de Modélisation et Simulation Multi Echelle, MSME FRE3160 CNRS, 5 bd Descartes, 77454 Marne-la-Vallée, France, christian.soize@univ-paris-est.fr*

Abstract

The drill-string dynamics is difficult to predict due to the nonlinearities and uncertainties involved in the problem. In this paper a stochastic computational model is proposed to model uncertainties in the bit-rock interaction model. To do so, a new strategy that uses the nonparametric probabilistic approach is developed to take into account model uncertainties in the bit-rock nonlinear interaction model. The mean model considers the main forces applied to the column such as the bit-rock interaction, the fluid-structure interaction and the impact forces. The nonlinear Timoshenko beam theory is used and the nonlinear dynamical equations are discretized by means of the finite element method.

Key words:
drill-string dynamics, bit-rock probabilistic model, nonlinear stochastic dynamics, nonparametric probabilistic approach.

1. Introduction

Drill-strings are slender structures used to dig into the rock in search of oil and their dynamics must be controlled to avoid failures [1]. A general vibration perspective of the oil and gas drilling process can be found in [2]. We are particulary concerned with a vertical drill-string that may reach some kilometers. When the drill-string is that long, it turns out that the vibration control is harder for the following reasons: the nonlinearities are important, the sensors may not work properly and uncertainties increase.

The drill-string is composed by thin tubes called drill-pipes that together measure some kilometers and some thicker tubes called drill-collars that together have some hundred meters. The region composed by the thicker tubes is called Bottom-Hole-Assembly (BHA). Figure 1 shows the general scheme of the system analyzed. The forces taken into account are the motor torque (as a constant rotational speed at the top Ω_x), the supporting force f_{hook}, the torque t_{bit} and force f_{bit} at the bit, the weight of the column, the fluid forces, the impact and rubbing between the column and the borehole, the forces due to the stabilizer, and also the elastic and kinetic forces due to the deformation and to the motion of the structure.

There are some ways to model the nonlinear dynamics of a drill-string, *e.g.* [3, 4, 5, 6, 7, 8, 9, 10]. These models are able to quantify some effects that occur in a drilling operation (such as the stick-slip oscillations) but they cannot predict correctly the dynamical response of a real system. This is explained since, first, the above models are too simple compared to the real system and, second, uncertainties are not taken into account. Each author uses a different approach to the problem: [3, 4] use a one-mode approximation to analyze the problem, [8, 9, 10] use the Euler-Bernoulli beam model with the Finite Element Method, while [6, 7] use the Cosserat theory.

A fluid-structure interaction that takes into account the drilling fluid that flows inside and outside the column is not considered in any of the above works. In the present paper, the fluid-structure interaction model proposed in [11] is employed in the analysis.

To model the column, the Timoshenko beam model is applied and the Finite Element Method is used to discretize the system. Moreover, finite strains are considered with no simplifications (what couples axial, torsional and lateral vibrations).

In a drilling operation there are many sources of uncertainties such as material properties (column and drilling fluid), dimensions of the system (especially the borehole), fluid-structure interaction and bit-rock interaction. The uncertainty analysis of the present paper is focused on the bit-rock interaction because it seems to be one of the most important sources of uncertainties in this problem. There are few articles treating the stochastic problem of the drill-string dynamics, in especial we may cite [12, 13]. In [12], stochastic lateral forces are analyzed at the bit, and in [13], a random weight-on-bit is analyzed using a simple two degrees of freedom drill-string model.

The bit-rock interaction model used in the analysis is the one developed

in [7]. This model is able to reproduce the main phenomena and describes the penetration of the bit into the rock. Thus, it allows the analysis of the rate of penetration (ROP). Usually, the bit is assumed to be fixed [9, 10] or an average rate of penetration is assumed [14, 5].

The nonparametric probabilistic approach [15, 16, 17] is used to model the uncertainties in the bit-rock interaction, which is represented by a nonlinear operator. It should be noticed that a new strategy is developed to take into account uncertainties for a local nonlinear operator.

The paper is organized as follows. In Section 2 the mean model is presented then, in Section 3, the probabilistic model of the bit-rock interaction model is developed. The results are shown in Section 4 and the concluding remarks are made in Section 5.

2. Mean model

In this Section the equations used to model the problem are presented. The strategy used in this work is, in some respects, similar to the one used in [9], but there are several important additional features, such as (1) impact and rubbing between the column and the borehole, (2) shear (Timoshenko beam model), (3) fluid-structure interaction and (4) a bit-rock interaction model that allows the simulation of the bit penetration.

To derive the equations of motion, the extended Hamilton Principle is applied. Defining the potential Π by

$$\Pi = \int_{t_1}^{t_2} (U - T - W) dt \,, \tag{1}$$

where U is the potential strain energy, T is the kinetic energy and W is the work done by the nonconservative forces and any force not accounted in the potential energy. The first variation of Π must vanish:

$$\delta\Pi = \int_{t_1}^{t_2} (\delta U - \delta T - \delta W) dt = 0 \,. \tag{2}$$

2.1. Finite element discretization

In the discretization by means of the Finite Element Method a two-node approximation with six degrees of freedom per node is chosen (see Fig. 2). The nodal displacement is written as

$$u_e = \mathbf{N}_u \mathbf{u}_e \quad , \quad v_e = \mathbf{N}_v \mathbf{u}_e \quad , \quad w_e = \mathbf{N}_w \mathbf{u}_e \,, \tag{3}$$

$$\theta_{xe} = \mathbf{N}_{\theta_x} \mathbf{u}_e \quad , \quad \theta_{y_e} = \mathbf{N}_{\theta_y} \mathbf{u}_e \quad , \quad \theta_{ze} = \mathbf{N}_{\theta_z} \mathbf{u}_e \,, \tag{4}$$

where $\mathbf{N}$ is the shape function (see Appendix A), u_e, v_e and w_e are the displacements in x, y and z directions, θ_{xe}, θ_{ye} and θ_{ze} are the rotations about the x, y and z-axis (see Fig. 2).
The element coordinate is $\xi = x/l_e$ and

$$\mathbf{u}_e = \begin{pmatrix} u_1 & v_1 & \theta_{z1} & w_1 & \theta_{y_1} & \theta_{x1} & u_2 & v_2 & \theta_{z2} & w_2 & \theta_{y_2} & \theta_{x2} \end{pmatrix}^T \,, \tag{5}$$

where $(\cdot)^T$ means transpose.

The Total Lagrangian formulation is used, the stress tensor is the second Piola-Kirchhoff tensor and finite strains are considered (Green-Lagrange strain tensor). We are assuming axi-symmetry about the x-axis, small lateral displacements (v and w) and small rotations (θ_y and θ_z), and a linear stress-strain relationship.

2.2. Kinetic energy

The kinetic energy is written as

$$T = \frac{1}{2} \int_0^L (\rho A \mathbf{v}^T \mathbf{v} + \rho \boldsymbol{\omega}^T [I_t] \boldsymbol{\omega}) \, dx \,, \tag{6}$$

where ρ is the mass density, A is the cross sectional area, L is the length of the column, $[I_t]$ is the cross sectional inertial matrix, $\mathbf{v}$ is the velocity vector and $\boldsymbol{\omega}$ the angular velocity vector. The three following quantities $\mathbf{v}$, $[I_t]$ and $\boldsymbol{\omega}$ are written as

$$\mathbf{v} = \begin{pmatrix} \dot{u} \\ \dot{v} \\ \dot{w} \end{pmatrix} \,, \; [I_t] = \begin{pmatrix} I_p & 0 & 0 \\ 0 & I & 0 \\ 0 & 0 & I \end{pmatrix} \,, \; \boldsymbol{\omega} = \begin{pmatrix} \dot{\theta}_x + \theta_y \dot{\theta}_z \\ \cos(\theta_x)\dot{\theta}_y - \sin(\theta_x)\dot{\theta}_z \\ \sin(\theta_x)\dot{\theta}_y + \cos(\theta_x)\dot{\theta}_z \end{pmatrix} \,, \tag{7}$$

where the time derivative (d/dt) is denoted by a superposed dot. The angular velocity $\boldsymbol{\omega}$ is derived by first rotating the inertial frame about the x-axis θ_x, then rotating the resulting frame about the y-axis θ_y and, finally, rotating the resulting frame about the z-axis θ_z. It is written in the inertial frame and it is assumed small rotations θ_y and θ_z. Developing the expression of the kinetic energy yields

$$T = \frac{1}{2} \int_0^L [\rho A (\dot{u})^2 + \rho A (\dot{v})^2 + \rho A (\dot{w})^2 +$$

$$+\rho I(\dot{\theta}_y)^2 + \rho I(\dot{\theta}_z)^2 + \rho I_p(\dot{\theta}_x)^2 + 2\rho I_p(\dot{\theta}_x\theta_y\dot{\theta}_z)]dx\,. \tag{8}$$

The first three terms of Eq. (8) are related to the translational inertia, the next three terms are related to the rotational inertia and the last term is the coupling term. In rotor-dynamics analysis the coupling term $(2\rho I_p(\dot{\theta}_x\theta_y\dot{\theta}_z))$ yields the gyroscopic matrix which does not introduce a nonlinearity into the system as $\dot{\theta}_x \sim cte$ (see, for instance, [18]). In our case this is not true, therefore, it yields a nonlinear formulation. The first variation of the kinetic energy, after integrating by parts in time, may be written as

$$\delta T = -\int_0^L \Big[\rho A\ddot{u}\delta u + \rho A\ddot{v}\delta v + \rho A\ddot{w}\delta w + \rho I\ddot{\theta}_y\delta\theta_y + \rho I\ddot{\theta}_z\delta\theta_z + \rho I_p\ddot{\theta}_x\delta\theta_x +$$
$$+ (\rho I_p(-\theta_y\ddot{\theta}_z\delta\theta_x - \dot{\theta}_y\dot{\theta}_z\delta\theta_x + \dot{\theta}_x\dot{\theta}_z\delta\theta_y - \dot{\theta}_x\dot{\theta}_y\delta\theta_z - \theta_y\ddot{\theta}_x\delta\theta_z))\Big]\,dx\,. \tag{9}$$

For convenience the energy is divided in two parts. The first one is

$$\delta T_1 = -\int_0^L \Big[\rho A(\ddot{u}\delta u + \ddot{v}\delta v + \ddot{w}\delta w) + \rho I(\ddot{\theta}_y\delta\theta_y + \ddot{\theta}_z\delta\theta_z) + \rho I_p\ddot{\theta}_x\delta\theta_x\Big]\,dx\,, \tag{10}$$

which yields the constant mass matrix $[M]$. The second part is

$$\delta T_2 = -\int_0^L \Big[(\rho I_p(-\theta_y\ddot{\theta}_z\delta\theta_x - \dot{\theta}_y\dot{\theta}_z\delta\theta_x + \dot{\theta}_x\dot{\theta}_z\delta\theta_y - \dot{\theta}_x\dot{\theta}_y\delta\theta_z - \theta_y\ddot{\theta}_x\delta\theta_z))\Big]\,dx\,, \tag{11}$$

which yields the vector $\mathbf{f}_{\text{ke}}$ that is incorporated in the nonlinear force vector $\mathbf{f}_{\text{NL}}$ (see Eq. (31)). Note that this force couples the axial, torsional and lateral motions.

2.3. Strain energy

The strain energy is given by

$$U = \frac{1}{2}\int_V \boldsymbol{\epsilon}^T\mathbf{S}dV\,, \tag{12}$$

where V is the domain of integration, $\boldsymbol{\epsilon} = (\epsilon_{xx} \;\; 2\gamma_{xy} \;\; 2\gamma_{xz})^T$ is the Green-Lagrange strain tensor and $\mathbf{S}$ is Second Piola-Kirchhoff tensor (written in Voigt notation). Substituting $\mathbf{S} = [D]\boldsymbol{\epsilon}$ and computing the first variation of the strain energy yields

$$\delta U = \int_V \delta\boldsymbol{\epsilon}^T \begin{pmatrix} E & 0 & 0 \\ 0 & k_sG & 0 \\ 0 & 0 & k_sG \end{pmatrix} \boldsymbol{\epsilon}dV\,. \tag{13}$$

The Timoshenko beam model (where the cross sectional area remains plane but not necessarily perpendicular to the neutral line, *i.e*, shear effects are considered) is used because it is more general than the Euler-Bernoulli model, what gives more flexibility for the applications. If there is no shear, the equations reduce to the Euler-Bernoulli model.

The components of the Green-Lagrange strain tensor may be written as

$$\begin{aligned}
\epsilon_{xx} &= \frac{\partial u_x}{\partial x} + \frac{1}{2}\left(\frac{\partial u_x}{\partial x}\frac{\partial u_x}{\partial x} + \frac{\partial u_y}{\partial x}\frac{\partial u_y}{\partial x} + \frac{\partial u_z}{\partial x}\frac{\partial u_z}{\partial x}\right) , \\
\gamma_{xy} &= \frac{1}{2}\left(\frac{\partial u_y}{\partial x} + \frac{\partial u_x}{\partial y} + \frac{\partial u_x}{\partial x}\frac{\partial u_x}{\partial y} + \frac{\partial u_y}{\partial x}\frac{\partial u_y}{\partial y} + \frac{\partial u_z}{\partial x}\frac{\partial u_z}{\partial y}\right) , \\
\gamma_{xz} &= \frac{1}{2}\left(\frac{\partial u_z}{\partial x} + \frac{\partial u_x}{\partial z} + \frac{\partial u_x}{\partial x}\frac{\partial u_x}{\partial z} + \frac{\partial u_y}{\partial x}\frac{\partial u_y}{\partial z} + \frac{\partial u_z}{\partial x}\frac{\partial u_z}{\partial z}\right) .
\end{aligned} \tag{14}$$

The displacements written in the undeformed configuration are

$$\begin{aligned}
u_x &= u - y\theta_z + z\theta_y , \\
u_y &= v + y(\cos(\theta_x) - 1) - z\sin(\theta_x) , \\
u_z &= w + z(\cos(\theta_x) - 1) + y\sin(\theta_x) ,
\end{aligned} \tag{15}$$

in which u, v and w are the displacements of the neutral line. Note that $\cos(\theta_x)$ and $\sin(\theta_x)$ have not been simplified in the above expression. Eq. (13) may be written as

$$\delta U = \int_V (E\delta\epsilon_{xx}\epsilon_{xx} + 4k_sG\delta\gamma_{xy}\gamma_{xy} + 4k_sG\delta\gamma_{xz}\gamma_{xz})dV . \tag{16}$$

The linear terms yield the stiffness matrix $[K]$ and the higher order terms yield the geometric stiffness matrix $[K_{\mathrm{g}}]$ and the vector $\mathbf{f}_{\mathrm{se}}$ that is incorporated in the nonlinear force vector $\mathbf{f}_{\mathrm{NL}}$ (see Eq. (31)). Note that due to the finite strain formulation, the axial, torsional and lateral vibrations are all coupled.

2.4. Impact and rubbing

The forces generated by the impact and rubbing between the column and the borehole are modeled by concentrated forces and torques. The radial

forces are modeled as an elastic force governed by the stiffness parameter k_{ip} [N/m] such that

$$F_{r\text{ip}} \begin{cases} = 0 & , \text{if } (r - R_{\text{ch}} - R_o) \leq 0 \\ = -k_{\text{ip}}(r - R_{\text{ch}} - R_o) & , \text{if } (r - R_{\text{ch}} - R_o) > 0 \end{cases} \tag{17}$$

where $r = \sqrt{v^2 + w^2}$, R_{ch} is the radius of the borehole and R_o is the outer radius of the column. The rubbing between the column and the borehole is simply modeled as a frictional torque governed by the frictional coefficient μ_{ip} and is such that

$$T_{x\text{ip}} \begin{cases} = 0 & , \text{if } (r - R_{\text{ch}} - R_o) \leq 0 \\ = -\mu_{\text{ip}} F_{r\text{ip}} R_o \operatorname{sign}(\dot{\theta}_x) & , \text{if } (r - R_{\text{ch}} - R_o) > 0 \end{cases} \tag{18}$$

where μ_{ip} is the frictional coefficient.

2.5. Fluid-structure interaction model

The drilling fluid (mud) is responsible for transporting the cuttings (drilled solids) from the bottom to the top to avoid clogging of the hole. It also plays an important role in cooling and stabilizing the system [19]. The rheological properties of the mud are complex, see [20] for instance. There is no doubt that the drilling fluid influences the dynamics of a drill-string, but solving the complete problem would be extremely expensive computationally. There are some works that are strictly concerned with the drilling fluid flow, *e.g* [21, 22, 23]. We use a linear fluid-structure coupling model similar to [24, 11]. In this simplified model there are the following hypotheses,

1. For the inside flow the fluid is taken as inviscid; for the outside as viscous.
2. The flow induced by the rotational speed about the x-axis is not considered in this first analysis.
3. The pressure varies linearly with x.

The element matrices are presented in Eq. (19). These equations are an extension and an adaptation of the model developed in [11].

$$
\begin{aligned}
[M_{\mathrm{f}}]^{(e)} &= \int_0^1 \left(M_{\mathrm{f}} + \chi\rho_{\mathrm{f}}A_o\right)\left(\mathbf{N}_w^T\mathbf{N}_w + \mathbf{N}_v^T\mathbf{N}_v\right)l_e d\xi\,,\\
[K_{\mathrm{f}}]^{(e)} &= \int_0^1 \left(-M_{\mathrm{f}}U_i^2 - A_i p_i + A_o p_o - \chi\rho_{\mathrm{f}}A_o U_o^2\right)\left(\mathbf{N'}_w^T\mathbf{N'}_w + \mathbf{N'}_v^T\mathbf{N'}_v\right)\frac{1}{l_e}d\xi +\\
&\quad + \int_0^1 \left(-A_i\frac{\partial p_i}{\partial x} + A_o\frac{\partial p_o}{\partial x}\right)\left(\mathbf{N}_{\theta_y}^T\mathbf{N}_{\theta_y} + \mathbf{N}_{\theta_z}^T\mathbf{N}_{\theta_z}\right)l_e d\xi\,,\\
[C_{\mathrm{f}}]^{(e)} &= \int_0^1 \left(-2M_{\mathrm{f}}U_i + 2\chi\rho_{\mathrm{f}}A_o U_o\right)\left(\mathbf{N}_{\theta_y}^T\mathbf{N}_{\theta_y} + \mathbf{N}_{\theta_z}^T\mathbf{N}_{\theta_z}\right)l_e d\xi +\\
&\quad + \int_0^1 \left(\frac{1}{2}C_{\mathrm{f}}\rho_{\mathrm{f}}D_o U_o + k\right)\left(\mathbf{N}_w^T\mathbf{N}_w + \mathbf{N}_v^T\mathbf{N}_v\right)l_e d\xi\,,\\
\mathbf{f}_{\mathrm{f}}^{(e)} &= \int_0^1 \left(M_{\mathrm{f}}g - A_i\frac{\partial p_i}{\partial x} - \frac{1}{2}C_{\mathrm{f}}\rho_{\mathrm{f}}D_o U_o^2\right)\mathbf{N}_u^T l_e d\xi\,.
\end{aligned}
\tag{19}
$$

in which, M_{f} is the fluid mass per unit length, ρ_{f} is the density of the fluid, $\chi = \dfrac{(D_{\mathrm{ch}}/D_o)^2+1}{(D_{\mathrm{ch}}/D_o)^2-1}$ (>1), D_{ch} is the borehole (channel) diameter, D_i, D_o are the inside and outside diameters of the column, U_i, U_o are the inlet and outlet flow velocities, p_i, p_o are the pressures inside and outside the drill-string, A_i, A_o are the inside and outside cross sectional area of the column, C_{f}, k are the fluid viscous damping coefficients.

As pointed out before, it is assumed that the inner and the outer pressures (p_i and p_o) vary linearly with x

$$p_i = (\rho_{\mathrm{f}}g)\,x + p_{\mathrm{cte}}\,, \tag{20}$$

$$p_o = \left(\rho_{\mathrm{f}}g + \frac{F_{fo}}{A_o}\right)x\,, \tag{21}$$

where p_{cte} is a constant pressure and F_{fo} is the frictional force due to the external flow given by

$$F_{fo} = \frac{1}{2}C_{\mathrm{f}}\rho_{\mathrm{f}}\frac{D_o^2U_o^2}{D_{\mathrm{h}}}\,. \tag{22}$$

In the above equation, D_h is the hydraulic diameter ($4A_\mathrm{ch}/S_\mathrm{tot}$) and S_tot is the total wetted area per unit length ($\pi D_\mathrm{ch}+\pi D_o$). Note that the reference pressure is $p_o|_{x=0} = 0$. Another assumption is that there is no head loss when the fluid passes from the drill-pipe to the drill-collar (and vice-versa). The head loss due to the change in velocity of the fluid at the bottom (it goes down and then up) is given by

$$h = \frac{1}{2g}(U_i - U_o)^2 \,. \tag{23}$$

If the geometry and the fluid characteristics are given, only the inlet flow at $x = 0$ can be controlled as the fluid speed is calculated using the continuity equation and the pressures are calculated using the Bernoulli equation.

Examining Eq. (19), it can be noticed that the fluid mass matrix is the usual added mass that, in our case, represents a significant value. For example, using representative values, the added mass is approximately 50% of the original mass, what changes the natural frequencies in about 20%.

The fluid stiffness matrix depends on the speed of the inside and outside flow as well as on the pressure and on the pressure derivatives. Analyzing the signs in the equation (Eq. 19) it can be noticed that the outside pressure tends to stabilize the system while the inside pressure and the flow tends to destabilize the system. The term $(-p_i A_i + p_o A_0)$ plays a major role on the stiffness of the system because, even though p_i is close to p_o, in the drill collar region (at the bottom) A_0 is around ten times A_i what turns the system stiffer at the bottom.

The fluid damping matrix depends on the flow velocity as well as on the viscous parameters of the fluid which have not well established values. A detailed analysis of the damping is not addressed in the present paper.

Finally, the fluid force vector $\mathbf{f}_\mathrm{f}$ is a constant axial force induced by the fluid and it is the only fluid force in the axial direction.

2.6. Bit-rock interaction model

The model used in this work is the one developed in [7], which can be written as

$$\begin{aligned} \dot{u}_\mathrm{bit} &= -a_1 - a_2 f_\mathrm{bit} + a_3 \omega_\mathrm{bit} \,, \\ t_\mathrm{bit} &= -\mathrm{DOC}\, a_4 - a_5 \,, \\ \mathrm{DOC} &= \frac{\dot{u}_\mathrm{bit}}{\omega_\mathrm{bit}} \,, \end{aligned} \tag{24}$$

where f_{bit} is the axial force (also called weight-on-bit), t_{bit} is the torque about the x-axis and $a_1, \ldots, a_5$ are positive constants that depend on the bit and rock characteristics as well as on the average weight-on-bit. Note that $\dot{u}_{\text{bit}}$ (=ROP) depends linearly on f_{bit} and on ω_{bit} (=$\dot{\theta}_{\text{bit}}$), and t_{bit} depends linearly on the depth-of-cut (DOC). Note also that these forces couple the axial and torsional vibrations. Equation (24) is rewritten as

$$\begin{aligned} f_{\text{bit}} &= -\frac{\dot{u}_{\text{bit}}}{a_2 Z(\omega_{\text{bit}})^2} + \frac{a_3 \omega_{\text{bit}}}{a_2 Z(\omega_{\text{bit}})} - \frac{a_1}{a_2}\,, \\ t_{\text{bit}} &= -\frac{\dot{u}_{\text{bit}} a_4 Z(\omega_{\text{bit}})^2}{\omega_{\text{bit}}} - a_5 Z(\omega_{\text{bit}})\,, \end{aligned} \tag{25}$$

where $Z(\omega_{\text{bit}})$ is the regularization function:

$$Z(\omega_{\text{bit}}) = \frac{\omega_{\text{bit}}}{\sqrt{(\omega_{\text{bit}})^2 + e^2}}\,. \tag{26}$$

Z is such that t_{bit} is continuous and when ω_{bit} approaches zero, t_{bit} and $\dot{u}_{\text{bit}}$ vanish. The regularization function is plotted in Fig. 3. Figure 4 shows how the torque varies with ω_{bit}.

The models usually applied for the bit-rock interaction are based on [14], see [5, 10, 9], for instance. In [10, 9] the bit can not move and the torque at the bit is essentially given by:

$$t_{\text{bit}} = \mu_{\text{bit}} f_{\text{bit}} \left[\tanh(\omega_{\text{bit}}) + \frac{\alpha_1 \omega_{\text{bit}}}{1 + \alpha_2 \omega_{\text{bit}}^2} \right]\,, \tag{27}$$

where μ_{bit} is a factor that depends on the bit cutting characteristics and α_1, α_2 are constants that depend on the rock properties. Figure 5 shows a comparison of the torque at the bit for the models given by Eqs. (25) and (27). It shows that they are close to each other for $f_{\text{bit}} = -100$ kN (value used in the simulations), $\alpha_1 = \alpha_2 = 1$ and $\mu_{\text{bit}} = 0.04$ (data used in [10]).

The response of the system is calculated in the prestressed configuration, therefore the initial reaction force at the bit must be subtracted in the expression of f_{bit}.

2.7. Boundary and initial conditions

As boundary conditions, the lateral displacements and the rotations about the y and z-axis are zero at the top. The lateral displacements at the bit are

also zero. A constant rotational speed about the x-axis Ω_x is imposed at the top.

To apply the boundary conditions above, the lines and rows corresponding to the mentioned degrees of freedom are eliminated from the full matrices and the forces corresponding to the imposed rotational speed at the top are considered in the right hand side of the equation.

In drilling operations there are stabilizers in the BHA region that help to decrease the amplitude of lateral vibrations. Stabilizers are considered as elastic elements:

$$F_y|_{x=x_{\text{stab}}} = k_{\text{stab}}\, v|_{x=x_{\text{stab}}} \quad \text{and} \quad F_z|_{x=x_{\text{stab}}} = k_{\text{stab}}\, w|_{x=x_{\text{stab}}}\,, \tag{28}$$

where x_{stab} is the stabilizer location and k_{stab} is the stabilizer stiffness.

As initial conditions, all the points move with constant axial speed and constant rotational speed about the x-axis, and the column is deflected laterally.

2.8. Initial prestressed configuration

Before starting the rotation about the x-axis, the column is put down through the channel until it reaches the soil. At this point the forces acting on the structure are: the reaction force at the bit, the weight of the column, the supporting force at the top and a constant fluid force. In this equilibrium configuration, the column is prestressed (see Fig. 6). There is tension above the neutral point and compression below it.
The initial prestressed state is calculated by:

$$\mathbf{u}_{\text{S}} = [K]^{-1}(\mathbf{f}_{\text{g}} + \mathbf{f}_c + \mathbf{f}_{\text{f}})\,. \tag{29}$$

where $\mathbf{f}_{\text{g}}$ is the gravity, $\mathbf{f}_c$ is the reaction force at the bit and $\mathbf{f}_{\text{f}}$ is the fluid axial force.

2.9. Final discretized system of equations

After assemblage and considering the prestressed configuration (Eq. (29)), the final discretized system is written as

$$([M]+[M_{\text{f}}])\ddot{\overline{\mathbf{u}}}+([C]+[C_{\text{f}}])\dot{\overline{\mathbf{u}}}+([K]+[K_{\text{f}}]+[K_{\text{g}}(\mathbf{u}_{\text{S}})])\overline{\mathbf{u}} = \mathbf{f}_{\text{NL}}(t, \overline{\mathbf{u}}, \dot{\overline{\mathbf{u}}}, \ddot{\overline{\mathbf{u}}})\,, \tag{30}$$

in which $\overline{\mathbf{u}} = \mathbf{u} - \mathbf{u}_{\text{S}}$. The response $\overline{\mathbf{u}}$ is represented in a subspace $V_m \subset \mathbb{R}^m$, where m equals the number of degrees of freedom of the system. $[M]$, $[C]$ and

$[K]$ are the usual mass, damping and stiffness matrices, $[M_\mathrm{f}]$, $[C_\mathrm{f}]$ and $[K_\mathrm{f}]$ are the fluid mass, damping and stiffness matrices, $\mathbf{f}_\mathrm{f}$ is the fluid force vector, $[K_\mathrm{g}(\mathbf{u}_\mathrm{S})]$ is the geometric stiffness matrix and $\mathbf{f}_\mathrm{NL}(t, \overline{\mathbf{u}}, \dot{\overline{\mathbf{u}}}, \ddot{\overline{\mathbf{u}}})$ is the nonlinear force vector that is written as

$$\mathbf{f}_\mathrm{NL}(t, \overline{\mathbf{u}}, \dot{\overline{\mathbf{u}}}, \ddot{\overline{\mathbf{u}}}) = \mathbf{f}_\mathrm{ke}(\overline{\mathbf{u}}, \dot{\overline{\mathbf{u}}}, \ddot{\overline{\mathbf{u}}}) + \mathbf{f}_\mathrm{se}(\overline{\mathbf{u}}) + \mathbf{f}_\mathrm{ip}(\overline{\mathbf{u}}) + \mathbf{f}_\mathrm{br}(\dot{\overline{\mathbf{u}}}) + \mathbf{g}(t)\,. \tag{31}$$

where $\mathbf{f}_\mathrm{ke}$ is composed by the quadratic terms of the kinetic energy (see Section 2.2), $\mathbf{f}_\mathrm{se}$ is composed by the quadratic and higher order terms of the strain energy (see Section 2.3), $\mathbf{f}_\mathrm{ip}$ is the force vector due to the impact and rubbing between the column and the borehole (see Section 2.4), $\mathbf{f}_\mathrm{br}$ is the force vector due to the bit-rock interactions (see Section 2.6) and $\mathbf{g}(t)$ is the force that corresponds to the Dirichlet boundary condition (rotational speed imposed at the top).

2.10. Reduced model

Usually the final discretized FE system have big matrices (dimension $m \times m$) and the dynamical analysis may be time consuming, which is the case of the present analysis. One way to reduce the system is to project the nonlinear dynamical equation on a subspace V_n, with $n << m$, in which V_n is spanned by an algebraic basis of $\mathbb{R}^n$. In the present paper, the basis used for the reduction corresponds to the normal modes projection. The normal modes are obtained from the following generalized eigenvalue problem

$$([K] + [K_\mathrm{f}] + [K_\mathrm{g}(\mathbf{u}_\mathrm{S})])\boldsymbol{\phi} = \omega^2([M] + [M_\mathrm{f}])\boldsymbol{\phi}\,, \tag{32}$$

where $\boldsymbol{\phi}_i$ is the i-th normal mode and ω_i is the i-th natural frequency. Using the representation

$$\overline{\mathbf{u}} = [\Phi]\,\mathbf{q}\,, \tag{33}$$

and substituting it in the Eq. (30) yields

$$([M]+[M_\mathrm{f}])[\Phi]\ddot{\mathbf{q}}+([C]+[C_\mathrm{f}])[\Phi]\dot{\mathbf{q}}+([K]+[K_\mathrm{f}]+[K_\mathrm{g}(\mathbf{u}_\mathrm{S})])[\Phi]\mathbf{q} = \mathbf{f}_\mathrm{NL}(t, \overline{\mathbf{u}}, \dot{\overline{\mathbf{u}}}, \ddot{\overline{\mathbf{u}}})\,. \tag{34}$$

where $[\Phi]$ is a $(m \times n)$ real matrix composed by n normal modes. Projecting Eq. (34) on the subspace spanned by these normal modes yields

$$[M_r]\,\ddot{\mathbf{q}}(t) + [C_r]\,\dot{\mathbf{q}}(t) + [K_r]\,\mathbf{q}(t) = [\Phi]^T\mathbf{f}_\mathrm{NL}(t, \overline{\mathbf{u}}, \dot{\overline{\mathbf{u}}}, \ddot{\overline{\mathbf{u}}})\,, \tag{35}$$

where

$$[M_r] = [\Phi]^T([M] + [M_{\rm f}])[\Phi], \quad [C_r] = [\Phi]^T([C] + [C_{\rm f}])[\Phi]\,,$$

$$[K_r] = [\Phi]^T([K] + [K_{\rm f}] + [K_{\rm g}(\mathbf{u}_{\rm S})])[\Phi] \tag{36}$$

are the reduced matrices.

3. Probabilistic model for the uncertain bit-rock interaction model

The parametric probabilistic approach allows physical-parameter uncertainties to be modeled. It should be noted that the underlying deterministic model defined by Eq. (25) exhibits parameters a_1, a_2, a_3, a_4 and a_5 which do not correspond to physical parameters. Consequently, it is difficult to construct an *a priori* probabilistic model using the parametric probabilistic approach. For instance, there is no available information concerning the statistical dependence of these parameters. Then, we propose to apply the nonparametric probabilistic approach to model uncertainties [15] which consists in modeling the operator of the constitutive equation (Eq. (25)) by a random operator. Such an approach allows both system-parameters uncertainties and modeling errors to be globally taken into account.

The nonparametric probabilistic approach has been applied for linear operators [17]. Recently it was extended [25] but the type of problem studied in the present paper is completely different from the geometrically nonlinear dynamical system studied in [25]. We are dealing with a nonlinear operator (related to a local nonlinearity). Therefore, it requires a different methodology. Let $\mathfrak{f}_{\rm bit}(\dot{\mathbf{x}})$ and $\dot{\mathbf{x}}$ be such that

$$\mathfrak{f}_{\rm bit}(\dot{\mathbf{x}}) = \begin{pmatrix} f_{\rm bit}(\dot{\mathbf{x}}) \\ t_{\rm bit}(\dot{\mathbf{x}}) \end{pmatrix} \quad \text{and} \quad \dot{\mathbf{x}} = \begin{pmatrix} \dot{u}_{\rm bit} \\ \omega_{\rm bit} \end{pmatrix}. \tag{37}$$

In the fist step of the methodology proposed, we look for a symmetric positive-definite matrix $[A_b(\dot{\mathbf{x}})]$ depending on $\dot{\mathbf{x}}$ such that the virtual power of the bit-rock interactions be written as

$$\delta\mathcal{P}_{\rm bit}(\dot{\mathbf{x}}) = \ < \mathfrak{f}_{\rm bit}(\dot{\mathbf{x}}), \delta\dot{\mathbf{x}} > \ = \ - < [A_b(\dot{\mathbf{x}})]\dot{\mathbf{x}}, \delta\dot{\mathbf{x}} >\,, \tag{38}$$

and such that force $\mathfrak{f}_{\rm bit}(\dot{\mathbf{x}})$ be given by:

$$\mathfrak{f}_{\rm bit}(\dot{\mathbf{x}}) = \nabla_{\delta\dot{\mathbf{x}}}\ \delta\mathcal{P}_{\rm bit}(\dot{\mathbf{x}})\,, \tag{39}$$

Equation (25) can be rewritten as

$$\mathfrak{f}_{\rm bit}(\dot{\mathbf{x}}) = -[A_b(\dot{\mathbf{x}})]\dot{\mathbf{x}} = -\begin{pmatrix} \dfrac{a_1}{a_2} + \dfrac{\dot{u}_{\rm bit}}{a_2 Z(\omega_{\rm bit})^2} - \dfrac{a_3\omega_{\rm bit}}{a_2 Z(\omega_{\rm bit})} \\ \dfrac{a_4 Z(\omega_{\rm bit})^2 \dot{u}_{\rm bit}}{\omega_{\rm bit}} + a_5 Z(\omega_{\rm bit}) \end{pmatrix} . \tag{40}$$

From Eqs. (38) to (40) it can be deduced that

$$\begin{aligned} [A_b(\dot{\mathbf{x}})]_{11} &= \frac{a_1}{a_2\dot{u}_{\rm bit}} + \frac{1}{a_2 Z(\omega_{\rm bit})^2} - \frac{a_3\omega_{\rm bit}}{a_2 Z(\omega_{\rm bit})\dot{u}_{\rm bit}} , \\ [A_b(\dot{\mathbf{x}})]_{22} &= \frac{a_4 Z(\omega_{\rm bit})^2 \dot{u}_{\rm bit}}{\omega_{\rm bit}^2} + \frac{a_5 Z(\omega_{\rm bit})}{\omega_{\rm bit}} , \\ [A_b(\dot{\mathbf{x}})]_{12} &= [A_b(\dot{\mathbf{x}})]_{21} = 0 . \end{aligned} \tag{41}$$

It can be seen that for all $\dot{\mathbf{x}}$ belonging to its admissible space $\mathcal{C}$, $[A_b(\dot{\mathbf{x}})]$ is positive-definite.

The second step consists, for all deterministic vector $\dot{\mathbf{x}}$ belonging to $\mathcal{C}$, in modeling matrix $[A_b(\dot{\mathbf{x}})]$ by a random matrix $[\mathbf{A}_b(\dot{\mathbf{x}})]$ with values in the set $\mathbb{M}_2^+(\mathbb{R})$ of all positive-definite symmetric (2×2) real matrices. Note that matrix $[\mathbf{A}_b(\dot{\mathbf{x}})]$ should be written as $[\mathbf{A}_b(\dot{\mathbf{x}}(t))]$ which shows that $\{[\mathbf{A}_b(\dot{\mathbf{x}}(t))], t > 0\}$ is a stochastic process with values in $\mathbb{M}_2^+(\mathbb{R})$. Thus, for all $\dot{\mathbf{x}}$ in $\mathcal{C}$, the constitutive equation defined by Eq. (40) becomes a random constitutive equation which can be written as

$$\mathfrak{F}_{\rm bit}(\dot{\mathbf{x}}) = -[\mathbf{A}_b(\dot{\mathbf{x}})]\dot{\mathbf{x}} . \tag{42}$$

The third step consists in constructing the probability distribution of random variable $[\mathbf{A}_b(\dot{\mathbf{x}})]$ for all fixed vector $\dot{\mathbf{x}}$ in $\mathcal{C}$. The available information is [17]:

1. Random matrix $[\mathbf{A}_b(\dot{\mathbf{x}})]$ is positive-definite almost surely,
2. $E\{[\mathbf{A}_b(\dot{\mathbf{x}})]\} = [A_b(\dot{\mathbf{x}})]$,
3. $E\{||[\mathbf{A}_b(\dot{\mathbf{x}})]^{-1}||_F^2\} = \mathrm{c}_1$, $|\mathrm{c}_1| < +\infty$,

in which $E\{\cdot\}$ is the mathematical expectation, $||\cdot||_F$ denotes the Frobenius norm such that $|||[A]|||_F = (tr\{[A][A]^T\})^{1/2}$ and $[A_b(\dot{\mathbf{x}})]$ is the matrix of the mean model. Following the methodology of the nonparametric probabilistic

approach and using the Cholesky decomposition, the mean value of $[A_b(\dot{\mathbf{x}})]$ is written as

$$[A_b(\dot{\mathbf{x}})] = [L_b(\dot{\mathbf{x}})]^T [L_b(\dot{\mathbf{x}})] \,, \tag{43}$$

and random matrix $[\mathbf{A}_b(\dot{\mathbf{x}})]$ is defined by

$$[\mathbf{A}_b(\dot{\mathbf{x}})] = [L_b(\dot{\mathbf{x}})]^T [\mathbf{G}_b][L_b(\dot{\mathbf{x}})] \,. \tag{44}$$

In the above equation, $[\mathbf{G}_b]$ is a random matrix satisfying the following available information:

1. Random matrix $[\mathbf{G}_b]$ is positive-definite almost surely,
2. $E\{[\mathbf{G}_b]\} = [\, I \,]$,
3. $E\{|||[\mathbf{G}_b]^{-1}||_F^2\} = \mathrm{c}_2$, $|\mathrm{c}_2| < +\infty$,

in which $[\, I \,]$ is the identity matrix. It should be noted that, in the construction proposed, random matrix $[\mathbf{G}_b]$ neither depends on $\dot{\mathbf{x}}$ nor on t. Let the dispersion parameter δ be such that

$$\delta = \left\{ \frac{1}{2} E\{|||[\mathbf{G_b}] - [I]||_F^2\} \right\}^{\frac{1}{2}} \,. \tag{45}$$

Taking into account the above available information and using the Maximum Entropy Principle [26, 27, 28] yield the following probability density function of $[\mathbf{G}_b]$ [17],

$$p_{[\mathbf{G}_b]}([G_b]) = \mathbb{1}_{\mathbb{M}_2^+(\mathbb{R})}([G_b]) C_{\mathbf{G}_b} \det([G_b])^{3\frac{(1-\delta^2)}{2\delta^2}} \exp\left\{ -\frac{3}{2\delta^2} \mathrm{tr}([G_b]) \right\}, \tag{46}$$

where $\det(\cdot)$ is the determinant, $\mathrm{tr}(\cdot)$ is the trace. The constant of normalization is written as

$$C_{\mathbf{G}_b} = \frac{\left(\frac{3}{2\delta^2}\right)^{3/(2\delta^2)}}{(2\pi)^{1/2} \Gamma\left(\frac{3}{2\delta^2}\right) \Gamma\left(\frac{3}{2\delta^2} - \frac{1}{2}\right)} \,, \tag{47}$$

where $\Gamma(z)$ is the gamma function defined for $z > 0$ by $\Gamma(z) = \int_0^{+\infty} t^{z-1} e^{-t} dt$.

The random generator of independent realizations of random matrix $[\mathbf{G}_b]$ for which the probability density function defined is by Eq. (46) is given in Appendix B. Deterministic Eqs. (30) and (31) are rewritten as

$$\mathcal{L}_{\mathrm{NL}}(\overline{\mathbf{u}}(t), \dot{\overline{\mathbf{u}}}(t), \ddot{\overline{\mathbf{u}}}(t)) = \mathbf{f}_{\mathrm{br}}(\dot{\overline{\mathbf{u}}}(t)) \,, \tag{48}$$

where $\mathcal{L}_{\rm NL}$ represents all the terms in Eqs. (30) and (31) except the bit forces $\mathbf{f}_{\rm br}$. The nonzero components of $\mathbf{f}_{\rm br}$ are related to the axial and torsional degrees of freedom at the bit and are represented by $\mathfrak{f}_{\rm bit}$ defined by Eq. (40). For stochastic modeling, $\mathfrak{f}_{\rm bit}$ is replaced by $\mathfrak{F}_{\rm bit}$ defined by Eq. (42). Consequently, Eq. (48) becomes a nonlinear stochastic differential equation which is such that

$$\mathcal{L}_{\rm NL}(\overline{\mathbf{U}}(t), \dot{\overline{\mathbf{U}}}(t), \ddot{\overline{\mathbf{U}}}(t)) = \mathbf{F}_{\rm br}(\dot{\overline{\mathbf{U}}}(t))\,, \tag{49}$$

where $\overline{\mathbf{U}}$ is the random response and $\mathbf{F}_{\rm br}$ is the random force at the bit that depends on $\mathfrak{F}_{\rm bit}(\dot{\mathbf{X}})$ in which $\dot{\mathbf{X}}$ is the random velocity vector of the bit and where $\mathfrak{F}_{\rm bit}(\dot{\mathbf{x}})$ is given by

$$\mathfrak{F}_{\rm bit}(\dot{\mathbf{x}}) = -[L_b(\dot{\mathbf{x}})]^T[\mathbf{G}_b][L_b(\dot{\mathbf{x}})]\dot{\mathbf{x}}\,. \tag{50}$$

For stochastic calculation, let

$$[\mathbf{G}_b(s_1)], \ldots, [\mathbf{G}_b(s_{n_s})] \tag{51}$$

be n_s independent realizations of random matrix $[\mathbf{G}_b]$. For each realization s_j $(j = 1, .., n_s)$, we have to solve the deterministic equation

$$\mathcal{L}_{\rm NL}(\overline{\mathbf{U}}(t, s_j), \dot{\overline{\mathbf{U}}}(t, s_j), \ddot{\overline{\mathbf{U}}}(t, s_j)) = \mathbf{F}_{\rm br}(\dot{\overline{\mathbf{U}}}(t, s_j), s_j)\,, \tag{52}$$

in which $\mathbf{F}_{\rm br}(\dot{\overline{\mathbf{U}}}(t, s_j), s_j)$ only depends on $\mathfrak{F}_{\rm bit}(\dot{\mathbf{X}}(t, s_j), s_j)$ which is calculated (see Eq. (50)) by

$$\mathfrak{F}_{\rm bit}(\dot{\mathbf{X}}(t, s_j), s_j) = -[L_b(\dot{\mathbf{X}}(t, s_j))]^T\,[\mathbf{G}_b(s_j)]\,[L_b(\dot{\mathbf{X}}(t, s_j))]\,\dot{\mathbf{X}}(t, s_j)\,. \tag{53}$$

4. Numerical results

The drill-string is discretized with 56 finite elements. For the construction of the reduced dynamical model, 158 lateral modes, 4 torsional modes, 3 axial modes and also the two rigid body modes of the structure (axial and torsional) are used. The columns of matrix $[\Phi]$ are made up of 167 modes. The number 167 has been chosen after several numerical experiments in order to get convergence. For the time integration procedure, the implicit Newmark integration scheme [29] has been implemented with a predictor and a fix point procedure to equilibrate the system response at each time step. The data used

for computations are representative values that are found in the literature [5, 7, 9, 10] (see Appendix C). All the numerical results presented below correspond to the forced response (deterministic case) and to the stationary response (stochastic case) for which the transient part of the response induced by the initial conditions has vanished. The results presented are the time response and the frequency spectrum defined as the modulus of its Fourier transform. The nonzero eigenfrequencies of the linearized system around the prestressed configuration (see Eq. 32) are given in Table 1. The lateral eigenfrequencies appear in pairs due to the symmetry about the x-axis.
The dynamical system is excited by a constant rotational speed about the x-axis at the top and with value 0.83 Hz. Note that for such an excitation, if there is no bit-rock interaction and no initial displacement in the lateral direction, there is no vibration in the forced response for the linearized system (there is only a rigid body displacement in rotation). In the presence of the nonlinear bit-rock interaction and without initial displacement in the lateral direction, the forced response does not exhibit lateral vibration and there are only coupled torsional and axial vibrations with a broad frequency spectrum. The results presented below correspond to the case with the nonlinear bit-rock interaction and an initial displacement in the lateral direction. Consequently, the forced response exhibits coupled torsional, axial and lateral vibrations on a broad band frequency spectrum. In fact, due to the nonlinearities induced by the bit-rock interactions forces an by the geometrical nonlinearities the frequency spectrum exhibits responses on a broad band for all components of the displacements.

4.1. Convergence of the stochastic solution

Let $[\overline{\mathbf{U}}(t, s_j)]$ be the response of the stochastic dynamical system calculated for each realization s_j. The mean-square convergence analysis with respect to the number n_s of independent realizations is carried out studying the function $n_s \mapsto \text{conv}(n_s)$ defined by

$$\text{conv}(n_s) = \frac{1}{n_s} \sum_{j=1}^{n_s} \int_0^{t_f} ||\overline{\mathbf{U}}(t, s_j)||^2 dt \,. \tag{54}$$

where t_f is the simulation time. Figure 7 shows that the mean-square convergence is reached for 150 simulations.

4.2. Stochastic response

The stochastic response is computed for three values of δ which are 0.001, 0.01, 0.1. Figure 8 displays the random ROP for $\delta = 0.001$. This figure shows the response of the mean model together with the mean response of the stochastic model and the 95% envelope (which means that the confidence region is constructed with a probability level of 0.95). The upper and lower envelopes of the confidence region are calculated using the method of quantiles [30].

Fig. 8(b) shows that the dispersion of the random ROP is already significant in the high part of the frequency band. However, the stochastic response in the low part of the frequency band is robust for the level of uncertainties considered. Figure 9 shows the random weight-on-bit and torque-on-bit. It should be noted that, for each time t, the coefficients of variation of the random weight-on-bit and of the random torque-on-bit are small ($\sim 5 \times 10^{-3}$). Nevertheless, although this dispersion is small, it induces a significant dispersion on the stochastic response (~ 0.15 for the coefficient of variation of the random ROP, for instance). Figure 10 shows the random rotational speed of the bit and Fig. 11 shows the random radial displacement at $x = 700$ m (middle point of the drill pipe). It can be seen that the lateral vibrations are also affected by the probabilistic model of the bit-rock interaction.

As δ increases the stochastic response gets more uncertain with wider statistical envelopes. Figure 12 shows the random ROP and Fig. 13 shows the random rotational speed of the bit (ω_{bit}) for $\delta = 0.01$. Note that some other peaks appear in the frequency spectrum. Figure 14 shows the random radial displacement. As shown in Fig. 14(a), there are some realizations where impacts occur between the column and the borehole.

Figure 15 shows the random rotational speed of the bit for $\delta = 0.1$. It can be noted that, for this level of uncertainty, the dispersion of the stochastic response is significant for all the frequency band analyzed. Figure 16 shows some Monte Carlo realizations of the stochastic ROP. The arrows in Fig. 16 indicate that, for some realizations, the bit loses contact with the soil.

The probabilistic model proposed for the bit-rock interaction model allows us to simulate cases such as the bit losing contact with the soil and the column impacting the borehole. The nonparametric probabilistic approach permits both parameters and modeling errors to be taken into account for the bit-rock interaction model.

5. Concluding remarks

A computational nonlinear dynamical model taking into account uncertainties has been developed to simulate the drill-string dynamics and it has been shown to be well suited to describe the problem. A probabilistic model has been proposed to model uncertainties in the bit-rock interaction model. Since the parameters of the mean model of the bit-rock interaction do not correspond to physical parameters, these parameters are not adequate to the use of the parametric probabilistic approach. Then, the nonparametric probabilistic approach has been used. This corresponds to a completely novel approach to take into account model uncertainties in a nonlinear constitutive equation. Since the dynamical system is globally nonlinear, an adapted strategy has been developed to implement a stochastic solver.

The nonlinear Timoshenko beam model has been used and the main forces that affect the dynamics of the drill-string have been considered such as the bit-rock interaction, the fluid-structure interaction and the impact forces.

The parametric numerical analysis performed shows that the nonlinear dynamical responses of this type of mechanical system is very sensitive to uncertainties in the bit-rock interaction model. In addition, these uncertainties play an important role in the coupling between the axial responses and the torsional one, and consequently, play a role in the lateral responses.

6. ACKNOWLEDGEMENTS

The authors acknowledge the financial support of the Brazilian agencies CNPQ, CAPES and FAPERJ, and the French agency COFECUB (project CAPES-COFECUB 476/04).

A. Shape functions

Linear shape functions are used for the axial and torsional displacements and the shape functions for the lateral displacements are derived by calculating the static response of the beam [31, 32]:

$$\mathbf{N}_u = [(1-\xi) \quad 0 \quad 0 \quad 0 \quad 0 \quad 0 \quad \xi \quad 0 \quad 0 \quad 0 \quad 0 \quad 0]\,,$$

$$\mathbf{N}_v = [0 \quad N_{v1} \quad N_{v2} \quad 0 \quad 0 \quad 0 \quad 0 \quad N_{v3} \quad N_{v4} \quad 0 \quad 0 \quad 0]\,,$$

$$\mathbf{N}_w = [0 \quad 0 \quad 0 \quad N_{v1} \quad -N_{v2} \quad 0 \quad 0 \quad 0 \quad 0 \quad N_{v3} \quad -N_{v4} \quad 0]\,,$$

$$\mathbf{N}_{\theta_x} = [0 \quad 0 \quad 0 \quad 0 \quad 0 \quad (1-\xi) \quad 0 \quad 0 \quad 0 \quad 0 \quad 0 \quad \xi]\,,$$

$$\mathbf{N}_{\theta_y} = [0 \quad 0 \quad 0 \quad -N_{\theta 1} \quad N_{\theta 2} \quad 0 \quad 0 \quad 0 \quad 0 \quad -N_{\theta 3} \quad N_{\theta 4} \quad 0]\,,$$

$$\mathbf{N}_{\theta_z} = [0 \quad N_{\theta 1} \quad N_{\theta 2} \quad 0 \quad 0 \quad 0 \quad 0 \quad N_{\theta 3} \quad N_{\theta 4} \quad 0 \quad 0 \quad 0]\,,$$

where:

$$N_{v1} = \tfrac{1}{1+\varphi}\left(1 - 3\xi^2 + 2\xi^3 + \varphi\,(1-\xi)\right)\,,$$

$$N_{v2} = \tfrac{l_e}{1+\varphi}\left(\xi - 2\xi^2 + \xi^3 + \tfrac{\varphi}{2}\,(\xi - \xi^2)\right)\,,$$

$$N_{v3} = \tfrac{1}{1+\varphi}\left(3\xi^2 - 2\xi^3 + \varphi\xi\right)\,,$$

$$N_{v4} = \tfrac{l_e}{1+\varphi}\left(-\xi^2 + \xi^3 + \tfrac{\varphi}{2}\,(\xi^2 - \xi)\right)\,,$$

$$N_{\theta 1} = \tfrac{1}{(1+\varphi)l_e}\left(-6\xi + 6\xi^2\right)\,,$$

$$N_{\theta 2} = \tfrac{1}{1+\varphi}\left(1 - 4\xi + 3\xi^2 + \varphi\,(1-\xi)\right)\,,$$

$$N_{\theta 3} = \tfrac{1}{(1+\varphi)l_e}\left(6\xi - 6\xi^2\right)\,,$$

$$N_{\theta 4} = \tfrac{1}{1+\varphi}\left(-2\xi + 3\xi^2 + \varphi\xi\right)\,,$$

in which $\varphi = \dfrac{12EI}{k_s G A l_e^2}$. Where E is the elasticity modulus, I is the area moment of inertia (y-z plane), k_s is shearing factor, G is the shear modulus, A is the cross sectional area and l_e is the length of an element.

B. Algorithm for the realizations of the random germ [G]

Random matrix $[\mathbf{G}]$ can be written as $[\mathbf{G}] = [\mathbf{L}_G]^T[\mathbf{L}_G]$ in which $[\mathbf{L}_G]$ is an upper triangular real random matrix such that:

1. The random variables $\{[\mathbf{L}_G]_{jj'}, j \leq j'\}$ are independents.
2. For $j < j'$ the real-valued random variable $[\mathbf{L}_G]_{jj'} = \sigma V_{jj'}$, in which $\sigma = \delta 3^{-1/2}$ and $V_{jj'}$ is a real-valued gaussian random variable with zero mean and unit variance.
3. For $j = j'$ the real-valued random variable $[\mathbf{L}_G]_{jj} = \sigma(2V_j)^{1/2}$. In which V_j is a real-valued gamma random variable with probability density function written as
$p_{V_j}(v) = \mathbb{1}_{\mathbb{R}^+}(v) \, \frac{1}{\Gamma\left(\frac{3}{2\delta^2}+\frac{1-j}{2}\right)} \; v^{\frac{3}{2\delta^2}-\frac{1+j}{2}} \; e^{-v}$.

C. Data used in the simulation

$\Omega_x = 0.83$ Hz (rotational speed about the x-axis at the top),
$L_{\text{dp}} = 1400$ m (length of the drill pipe),
$L_{\text{dc}} = 200$ m (length of the drill collar),
$D_{o\text{dp}} = 0.127$ m (outside diameter of the drill pipe),
$D_{o\text{dc}} = 0.2286$ m (outside diameter of the drill collar),
$D_{i\text{dp}} = 0.095$ m (inside diameter of the drill pipe),
$D_{i\text{dc}} = 0.0762$ m (inside diameter of the drill collar),
$D_{\text{ch}} = 0.3$ m (diameter of the borehole (channel)),
$x_{\text{stab}} = 1400$ m (location of the stabilizer),
$k_{\text{stab}} = 17.5$ MN/m (stiffness of the stabilizer per meter),
$E = 210$ GPa (elasticity modulus of the drill string material),
$\rho = 7850$ kg/m^3 (density of the drill string material),
$\nu = 0.29$ (poisson coefficient of the drill string material),
$k_s = 6/7$ (shearing correcting factor),
$k_{\text{ip}} = 1 \times 10^8$ N/m (stiffness per meter used for the impacts),
$\mu_{\text{ip}} = 0.0005$ (frictional coefficient between the string and the borehole),
$u_{in} = 1.5$ m/s (flow speed in the inlet),
$\rho_{\text{f}} = 1200$ kg/m^3 (density of the fluid),
$C_{\text{f}} = 0.0125$ (fluid viscous damping coefficient),
$k = 0$ (fluid viscous damping coefficient),
$g = 9.81$ m/s^2 (gravity acceleration),
$a_1 = 3.429 \times 10^{-3}$ m/s (constant of the bit-rock interaction model),

$a_2 = 5.672 \times 10^{-8}$ m/(N.s) (constant of the bit-rock interaction model),
$a_3 = 1.374 \times 10^{-4}$ m/rd (constant of the bit-rock interaction model),
$a_4 = 9.537 \times 10^{6}$ N.rd (constant of the bit-rock interaction model),
$a_5 = 1.475 \times 10^{3}$ N.m (constant of the bit-rock interaction model),
$e = 2$ rd/s (regularization parameter).

The damping matrix is constructed using the relationship $[C] = \alpha([M] + [M_{\mathrm{f}}]) + \beta([K] + [K_{\mathrm{f}}] + [K_{\mathrm{g}}(\mathbf{u}_{\mathrm{S}})])$ with $\alpha = 0.01$ and $\beta = 0.0003$.

References

[1] K. A. Macdonald and J. V. Bjune, Failure analysis of drillstrings, Engineering Failure Analysis, 14 (2007) 1641–1666.

[2] P. D. Spanos and A. M. Chevallier and N. P. Politis and M. L. Payne, Oil and Gas Well Drilling: A Vibrations Perspective, The Shock and Vibration Digest, 35 (2) (2003) 85-103.

[3] A. Yigit and A. Christoforou, Coupled axial and transverse vibrations of oilwell drillstrings, Journal of Sound and Vibration, 195 (4) (1996) 617-627.

[4] A. P. Christoforou and A. S. Yigit, Dynamic modeling of rotating drillstrings with borehole interactions, Journal of Sound and Vibration, 206 (2) (1997) 243-260.

[5] A. P. Christoforou and A. S. Yigit, Fully vibrations of actively controlled drillstrings, Journal of Sound and Vibration, 267 (2003) 1029-1045.

[6] R. W. Tucker and C. Wang, An integrated model for drill-string dynamics, Journal of Sound and Vibration, 224 (1) (1999) 123-165.

[7] R. W. Tucker and C. Wang, Torsional vibration control and cosserat dynamics of a drill-rig assembly, Meccanica, 224 (1) (2003) 123-165.

[8] Y.A. Khulief and H. Al-Naser, Finite element dynamic analysis of drillstrings, Finite Elements in Analysis and Design, 41 (2005) 1270-1288.

[9] Y.A. Khulief and F. A. Al-Sulaiman and S. Bashmal, Vibration analysis of drillstrings with self excited stick-slip oscillations, Journal of Sound and Vibration, 299 (2007) 540-558.

[10] R. Sampaio and M. T. Piovan and G. V. Lozano, Coupled axial/torsional vibrations of drilling-strings by mean of nonlinear model, Mechanics Research Comunications, 34 (5-6) (2007) 497-502.

[11] M. P. Paidoussis and T. P. Luu and S. Prabhakar, Dynamics of a long tubular cantilever conveying fluid downwards, which then flows upwards around the cantilever as a confined annular flow, Journal of Fluids and Structures, 24 (11) (2007) 111-128.

[12] P. D. Spanos, A. M. Chevallier and N.P. Politis, Nonlinear stochastic drill-string vibrations, Journal of Vibration and Acoustics, 124 (4) (2002) 512-518.

[13] S. J. Kotsonis and P. D. Spanos, Chaotic and random whirling motion of drillstrings, Journal of Energy Resources Technology (Transactions of the ASME), 119 (4) (1997) 217-222.

[14] P. D. Spanos and A. K. Sengupta and R. A. Cunningham and P. R. Paslay, Modeling of roller cone bit lift-off dynamics in rotary drilling, Journal of Energy Resources Technology, 117(3) (1995) 197-207.

[15] C. Soize, A nonparametric model of random uncertities for reduced matrix models in structural dynamics, Probabilistic Engineering Mechanics, 15 (2000) 277-294.

[16] C. Soize, Maximum entropy approach for modeling random uncertainties in trasient elastodynamics, Journal of the Acoustical Society of America, 109 (5) (2001) 1979-1996.

[17] C. Soize, Random matrix theory for modeling uncertainties in computational mechanics, Computer Methods in Applied Mechanics and Engineering, 194 (12-16) (2005) 1333-1366.

[18] D. Childs, Turbomachinery Rotordynamics: Phenomena, Modeling, and Analysis, Wiley-Interscience, 1993.

[19] ASME, Handbook: Drilling fluids processing, Elsevier Inc., 2005.

[20] P. Coussot and F. Bertrand and B. Herzhaft, Rheological Behavior of drilling muds, characterization using MRI vizualization, Oil and Gas Science and Technology, 59 (1) (2004) 23-29.

[21] M. P. Escudier and I. W. Gouldson and P. J. Oliveira and F. T. Pinho, Effects of inner cylinder rotation on laminar flow of a Newtonian Fuid through an eccentric annulus, International Journal of Heat and Fluid Flow, 21 (2000) 92-103.

[22] M. P. Escudier and P. J. Oliveira and F. T. Pinho, Fully developed laminar flow of purely viscous non-Newtonian liquids through annuli, including the effects of eccentricity and inner-cylinder rotation, International Journal of Heat and Fluid Flow, 23 (2002) 52-73.

[23] E. P. F. Pina and M. S. Carvalho, Three-Dimensional Flow of a Newtonian Liquid Through an Annular Space with Axially Varying Eccentricity, Journal of Fluids Engineering, 128 (2) (2006) 223-231.

[24] M. P. Paidoussis, Non-linear dynamics of a fluid-conveying cantilevered pipe with a small mass attached at the free end, International Journal of Non-Linear Mechanics, 33 (1) (1998) 15-32.

[25] M. P. Mignolet and C. Soize, Stochastic Reduced Order Models For Uncertain Geometrically Nonlinear Dynamical Systems, Computer Methods in Applied Mechanics and Engineering, 197 (45-48) (2008) 3951-3963.

[26] C. E. Shannon, A mathematical theory of communication, Bell System Tech. J., 27 (1948) 379-423 and 623-659.

[27] E. Jaynes, Information theory and statistical mechanics, The Physical Review, 106 (4) (1957) 1620-630.

[28] E. Jaynes, Information theory and statistical mechanics II, The Physical Review, 108 (1957) 171-190.

[29] K. J. Bathe, Finite Element Procedures, Prentice-Hall Inc., 1996.

[30] R. J. Serfling, Approximation Theorems of Mathematical Statistics, John Wiley & Sons, 1980.

[31] H. D. Nelson, A finite rotating shaft element using Timoshenko been theory, Journal of Mechanical Design, 102 (1980) 793-803.

[32] A. Bazoune and Y.A. Khulief, Shape functions of the three-dimensional Timoshenko beam element, Journal of Sound and Vibration, 259 (2) (2002) 473-480.

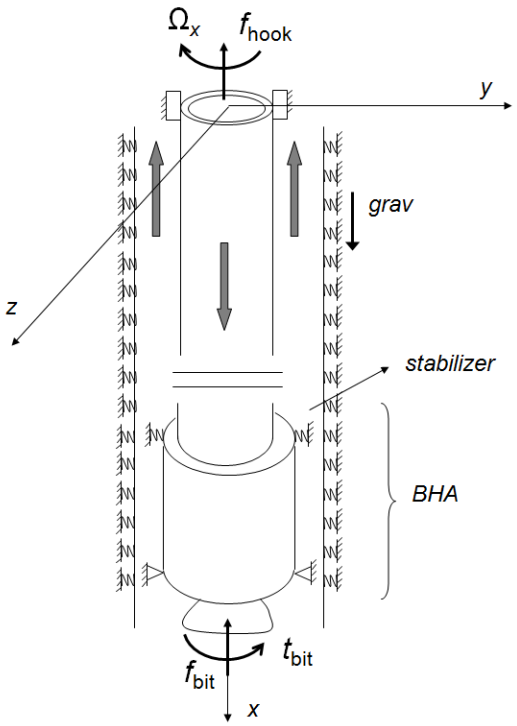

Figure 1: General scheme of the drill-string system.

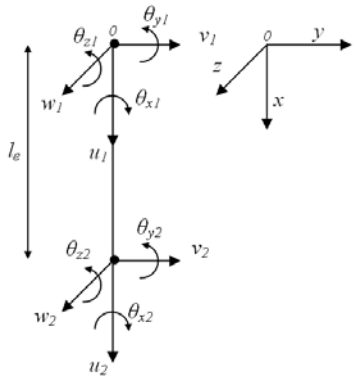

Figure 2: Degrees of freedom of an element.

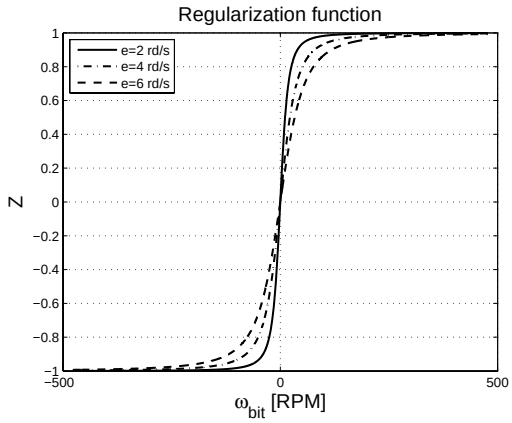

Figure 3: Regularization function.

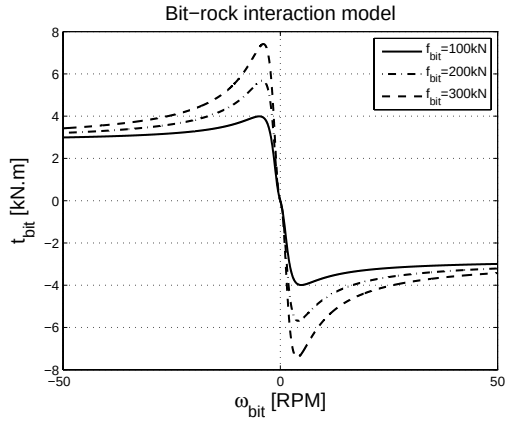

Figure 4: Torque at the bit in function of ω_{bit}.

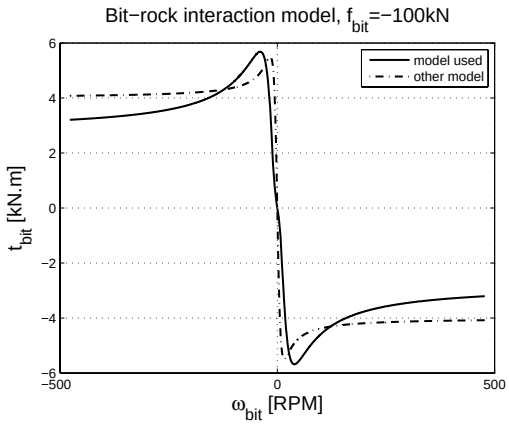

Figure 5: Torque at the bit in function of ω_{bit}.

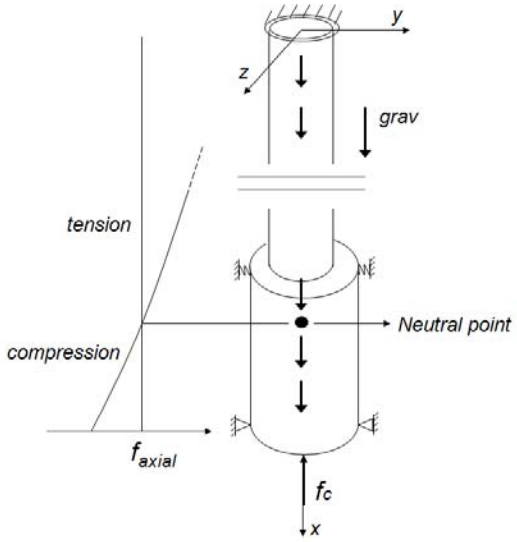

Figure 6: Initial prestressed configuration of the system.

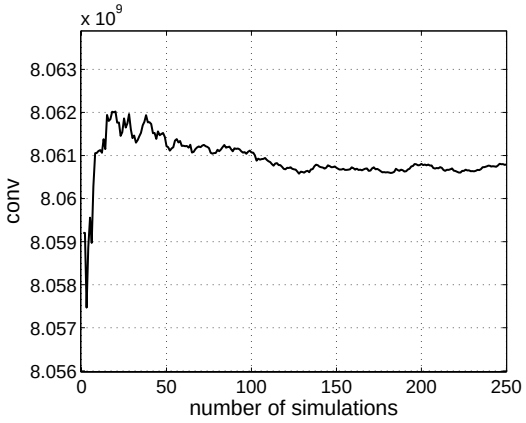

Figure 7: Typical mean square convergence curve.

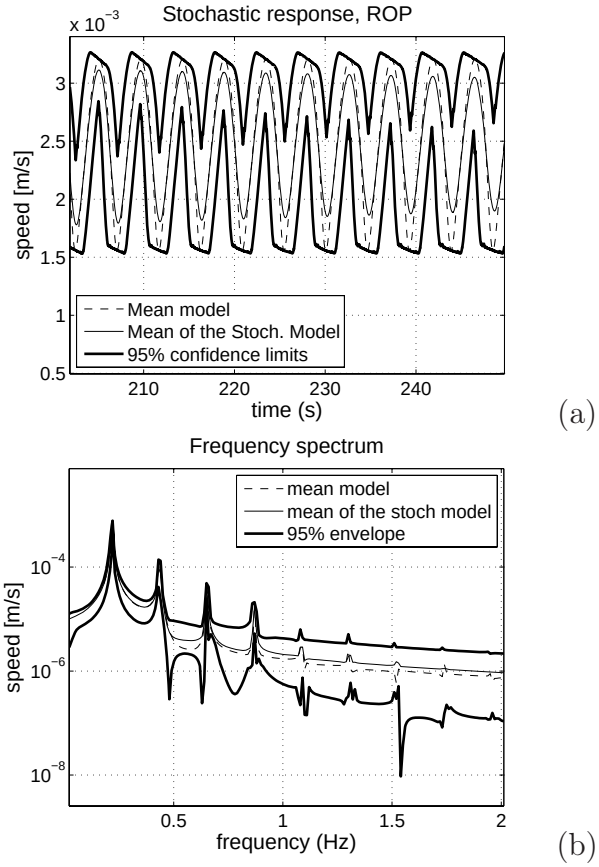

Figure 8: Stochastic response for $\delta = 0.001$. ROP (a) and its frequency spectrum (b).

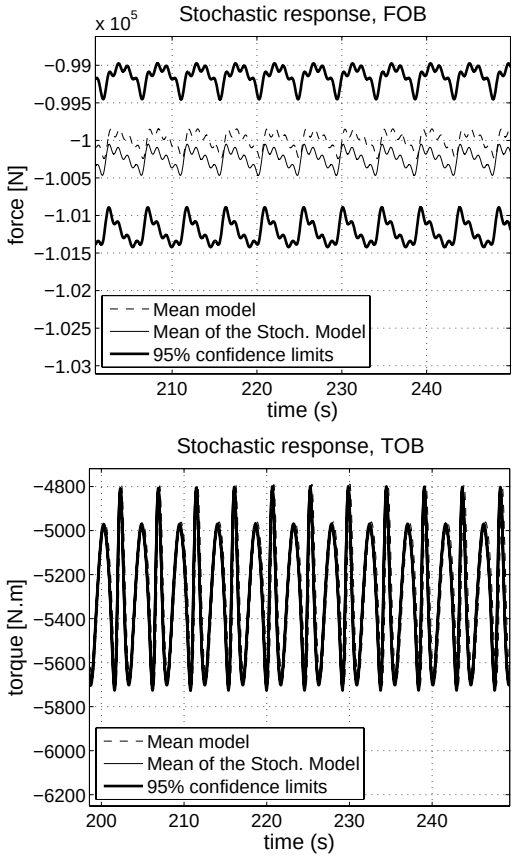

Figure 9: Stochastic response for $\delta = 0.001$. (a) weight-on-bit, (b) torque-on-bit.

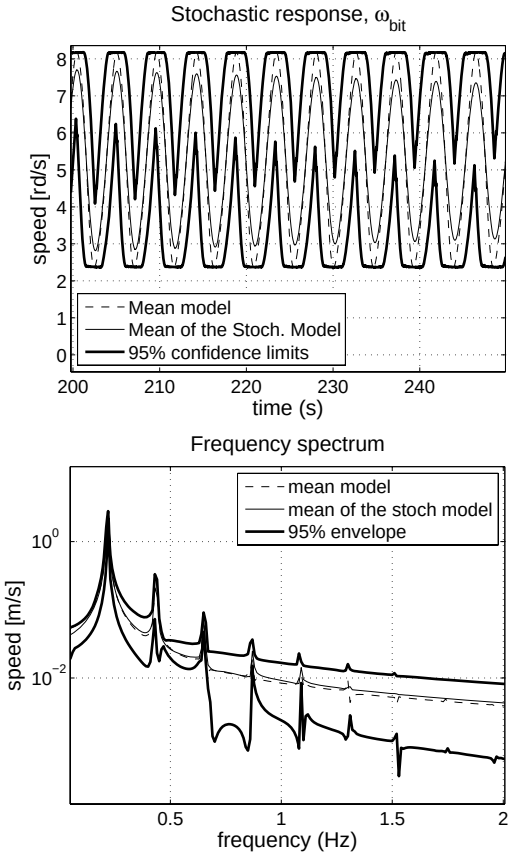

Figure 10: Stochastic response for $\delta = 0.001$. Rotational speed of the bit (a) and its frequency spectrum (b).

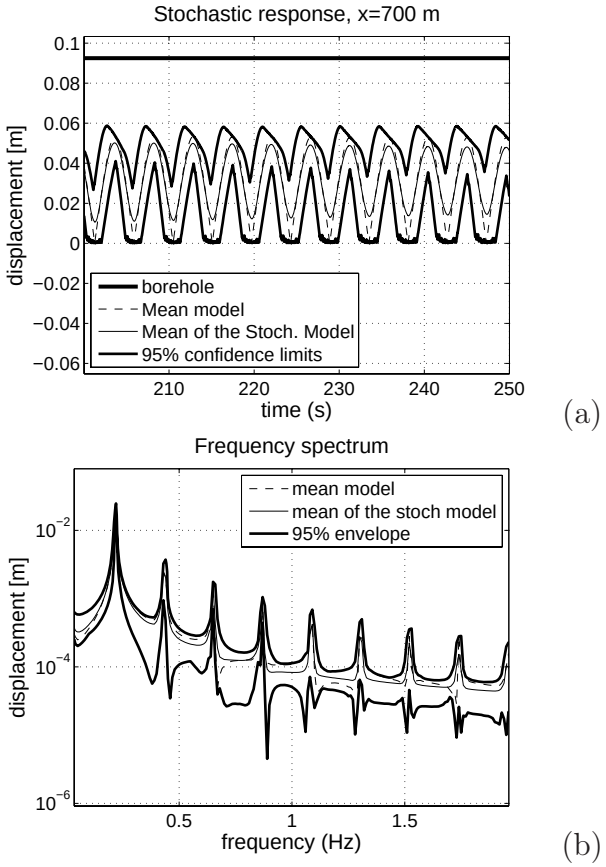

Figure 11: Stochastic response for $\delta = 0.001$. Radial displacement at $x = 700$ m (a) and its frequency spectrum (b).

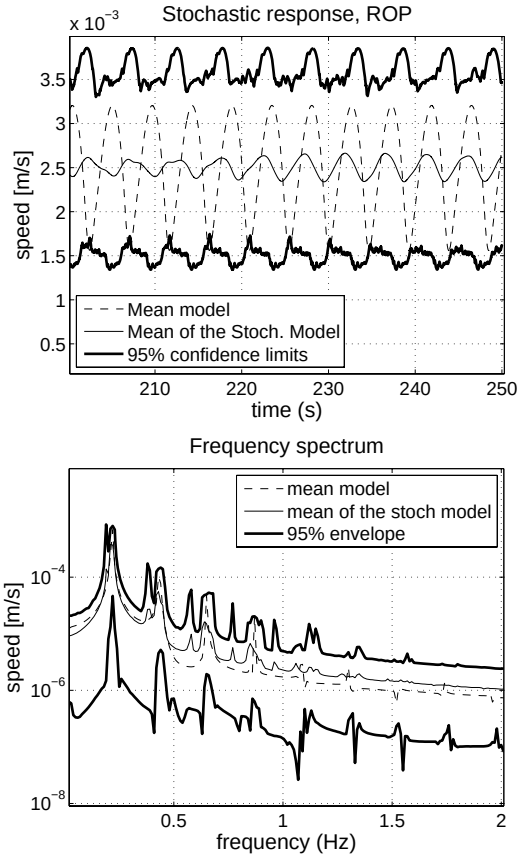

Figure 12: Stochastic response for $\delta = 0.01$. ROP (a) and its frequency spectrum (b).

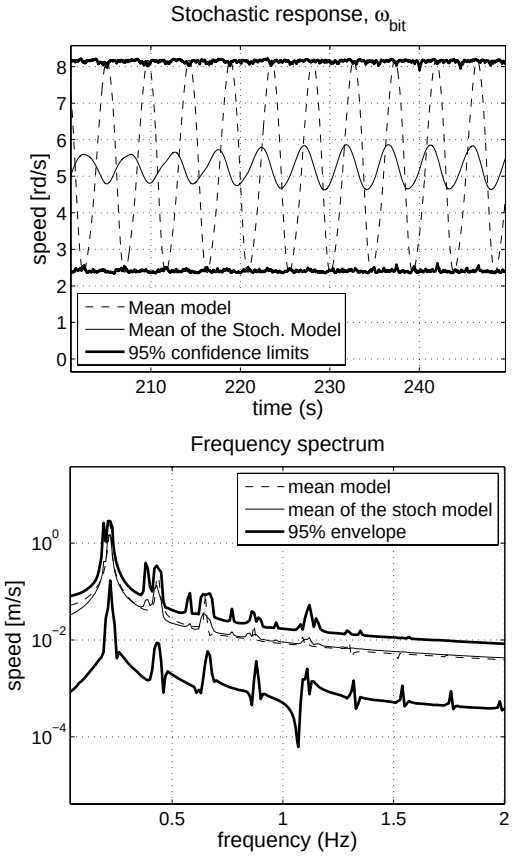

Figure 13: Stochastic response for $\delta = 0.01$. Rotational speed of the bit ω_{bit} (a) and its frequency spectrum (b).

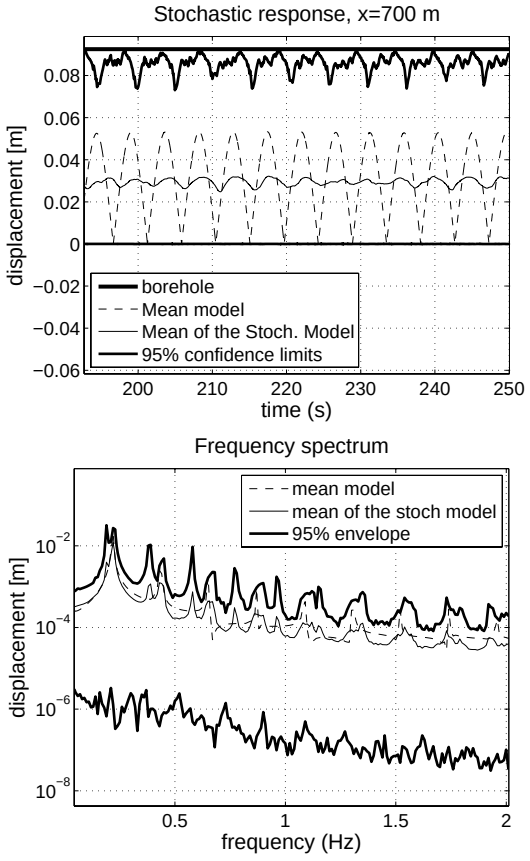

Figure 14: Stochastic response for $\delta = 0.01$. Radial displacement at $x = 700$ m and its frequency spectrum (b).

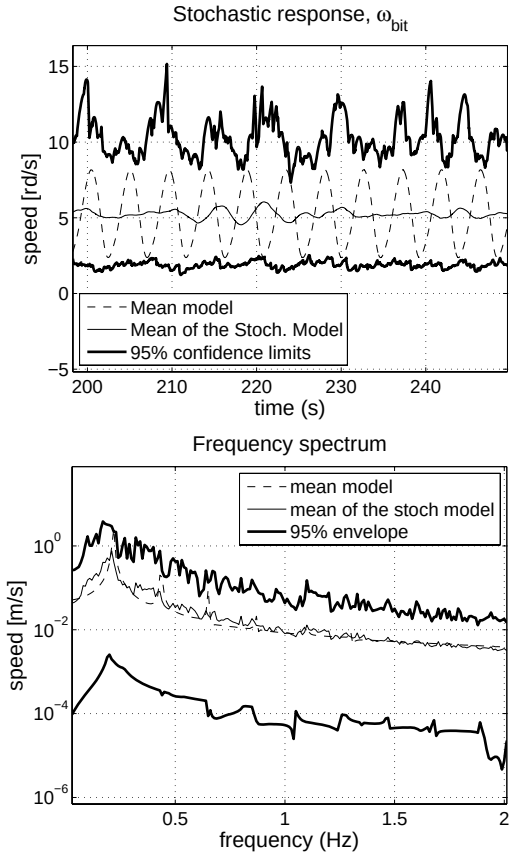

Figure 15: Stochastic response for $\delta = 0.1$. Rotational speed of the bit ω_{bit} (a) and its frequency spectrum (b).

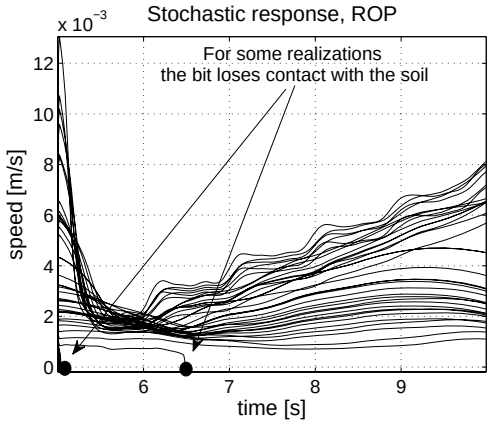

Figure 16: Random ROP for $\delta = 0.1$.

Rank	Eigenfrequency	Type
1-2	0.0372 Hz	Lateral
3-4	0.0744 Hz	Lateral
5-6	0.1065 Hz	Lateral
7-8	0.1117 Hz	Lateral
9-10	0.1488 Hz	Lateral
11-12	0.1860 Hz	Lateral
13	0.2144 Hz	Torsional
14-15	0.2160 Hz	Lateral
16-17	0.2234 Hz	Lateral
18-19	0.2605 Hz	Lateral
...	...	...
76	1.1105 Hz	Torsional
...	...	...
81	1.2018 Hz	Axial
...	...	...
163-164	3.2671 Hz	Lateral
165	4.6761 Hz	Axial

Table 1: Eigenfrequencies of the linearized system.